Accepted version

The final version of this manuscript has been published in:

International Journal of Pharmaceutics 2020, 589, 119881.

In vivo assessment of aminopeptidase N (APN/CD13) specificity of different ^{68}Ga-labelled NGR derivatives using PET/MRI imaging

Adrienn Kis[a,b], Noémi Dénes[a,c], Judit P. Szabó[a,b], Viktória Arató[a], István Jószai[a], Kata Nóra Enyedi[d], Szilvia Lakatos[a], Ildikó Garai[a,e], Gábor Mező[d,f], István Kertész[a,#], György Trencsényi[a,b,c,#*]

[a]Division of Nuclear Medicine and Translational Imaging, Department of Medical Imaging, Faculty of Medicine, University of Debrecen, Hungary;

[b]Doctoral School of Clinical Medicine, Faculty of Medicine, University of Debrecen, Nagyerdei St. 98, H-4032 Debrecen, Hungary

[c]Gyula Petrányi Doctoral School of Allergy and Clinical Immunology, Faculty of Medicine, University of Debrecen, Nagyerdei St. 98, H-4032 Debrecen, Hungary

[d]Eötvös Loránd University, Faculty of Science, Institute of Chemistry, Budapest, Hungary

[e]Scanomed LTD, Nagyerdei St. 98, H-4032 Debrecen, Hungary

[f]MTA-ELTE, Research Group of Peptide Chemistry, Hungarian Academy of Sciences, Eötvös L. University, Budapest, Hungary

# these authors contributed equally to the study

* corresponding author

Corresponding author:
György Trencsényi, PhD,
Division of Nuclear Medicine and Translational Imaging, Department of Medical Imaging, Faculty of Medicine, University of Debrecen, 4032, Debrecen, Nagyerdei krt. 98. Debrecen, Hungary,
E-mail: trencsenyi.gyorgy@med.unideb.hu

Abstract

Aminopeptidase N (APN/CD13) plays an important role in neoangiogenic process in malignancies. Our previous studies have already shown that ^{68}Ga-labelled NOTA conjugated asparagine-glycine-arginine peptide (c[KNGRE]-NH_2) specifically bind to APN/CD13 expressing tumors. The aim of this study was to evaluate and compare the APN/CD13 specificity of newly synthesized ^{68}Ga-labelled NGR derivatives *in vivo* by PET/MRI imaging using hepatocellular carcinoma (He/De) and mesoblastic nephroma (Ne/De) tumor models. PET/MRI and *ex vivo* biodistribution studies were performed 11±1 days after subcutaneous injection of tumor cells and 90 min after intravenous injection of ^{68}Ga-NOTA-c(NGR), ^{68}Ga-NODAGA-c(NGR), ^{68}Ga-NODAGA-c(NGR) (MG1) or ^{68}Ga-NODAGA-c(NGR) (MG2). The APN/CD13 selectivity was confirmed by blocking experiments and the APN/CD13 expression was verified by immunohistochemistry. ^{68}Ga-labelled c(NGR) derivatives were produced with high specific activity and radiochemical purity. In control animals, low radiotracer accumulation was found in abdominal and thoracic organs. Using tumor-bearing animals we found that the ^{68}Ga-NOTA-c(NGR), ^{68}Ga-NODAGA-c(NGR), and ^{68}Ga-NODAGA-c(NGR) (MG1) derivatives showed higher uptake in He/De and Ne/De tumors, than that of the accumulation of ^{68}Ga-NODAGA-c(NGR) (MG2). APN/CD13 is a very promising target in PET imaging, however, the selection of the appropriate ^{68}Ga-labelled NGR-based radiopharmaceutical is critical for the precise detection of tumor neo-angiogenesis and for monitoring the efficacy of anticancer therapy.

Keywords: aminopeptidase N, angiogenesis, CD13, ^{68}Ga, NGR, PET/MRI imaging

Abbreviations

APN/CD13: aminopeptidase N (CD13)

c(KNGRE)-NH_2: cyclic(lysyl-asparaginyl-glycyl-argininyl-glutamic acid amide)

He/De: rat hepatocellular carcinoma

MRI: magnetic resonance imaging

Ne/De: rat mesoblastic nephroma

NGR: asparaginyl-glycyl-arginine

NODAGA: 1,4,7-triazacyclononane,1-glutaric acid-4,7-acetic acid

NODAGA-c(NGR): c[Lys(NODAGA)-Asn-Gly-Arg-Glu]-NH_2

NODAGA-c(NGR) (MG1): c[CH_2-CO-Lys(NODAGA)-Asn-Gly-Arg-Cys]-NH_2

NODAGA-c(NGR) (MG2): c[CH_2-CO-Lys(NODAGA)-Asn-*N*(Me)Gly-Arg-Cys]-NH_2

NOTA: 1,4,7-triazacyclononane-triacetic acid

NOTA-c(NGR): c[Lys(NOTA)-Asn-Gly-Arg-Glu]-NH_2

PET: positron emission tomography

SUVmean: standardized uptake value (mean)

SUVmax: standardized uptake value (max)

T/M: tumor-to-muscle ratio

Chemical compounds studied in this article:

L-Arginine	CID: 6322
L-Asparagine	CID: 6267
N,*N*-dimethylformamide (DMF)	CID 6228
L-Glutamic acid	CID: 33032
Glyicine	CID: 750
1-hydroxybenzotriazole (HOBt)	CID 2796029
L-Lysine	CID: 5962
1,4,7-triazacyclononane-1,4,7-triacetic acid (NOTA)	CID 3036142
triflouroacetic acid (TFA)	CID 6422

1. Introduction

Neo-angiogenesis, as the new blood vessel formation from a pre-excist capillary system, plays an important role in several human diseases such as tumorigenesis (Folkman, 2002), heart failure (Higuchi et al., 2008), atherosclerosis and peripheral artery diseases (Carmeliet and Jain, 2000; Wu et al., 2013). The presence of neovascularization in malignant tumors is essential for tumor growth and progression, for the development of distant metastases and for the efficacy of antitumor therapies (Otsuki et al., 2018; Zheng et al., 2017; Zou et al., 2012). Increased expression of several molecules such as VEGF, integrins, endoglin, aminopeptidase N (APN)/CD13 (Deshpande et al., 2011; Máté et al., 2015) has been demonstrated in the membrane of cancer cells and tumor vascular endothelial cells during tumor growth, which play a pivotal role in tumor neo-angiogenesis. Furthermore, the specific targeting of these cell surface receptors greatly promote the diagnosis and therapy of malignancies (Jászai and Schmidt, 2019; Teleanu et al., 2019).

Among molecular targets of tumor neo-angiogenesis, APN/CD13 is one of the most promising molecules that serve as a potential target for tumor diagnosis and therapy. APN/CD13 is a Zn^{2+}-dependent transmembrane exopeptidase that - due to this enzyme catalyse the degradation of extracellular matrix - plays an important role in metastatic tumor cell invasion (Schreiber et al., 2018; Rundhaug, 2005). In addition APN/CD13 is being expressed in healthy organs and tissues (*e.g.*: epithelial cells of small intestine, kidney, in the synaptic membranes of central nervous system, smooth muscle cells), it is also expressed in tumor neovasculature and on the surface of several solid tumors, such as malignant melanoma, prostate, lung, pancreas and ovarian cancer (Chen et al., 2013; van Hensbergen et al., 2004; Otsuki et al., 2018).

Several studies reported that asparaginyl-glycyl-arginine (NGR) motif is a specific ligand of APN/CD13 (Corti et al., 2008; Enyedi et al., 2017), and it was found to be three times as efficient at the detection of neoangiogenic vessels than the widely used RGD (arginyl-glycyl-aspartic acid) peptides (Buehler et al., 2006). Several linear and cyclic NGR peptides have been developed and optimized, and it was found, that only a few NGR peptides (e.g.: [CNGRC] and [KNGRE]-NH_2) have shown the ability to target both tumors and new blood vessels with high specificity (Colombo et al., 2002; Negussie et al., 2010; Pasqualini et al., 2000). Furthermore, the small cyclic NGR peptides are superior in APN/CD13 specificity than that of the linear forms due to the conformational constraining cyclization (Enyedi et al., 2017).

Due to [KNGRE]-NH_2 peptide showed more favorable chemical stability properties, this NGR probe has been studied for several tumor targeting applications, such as positron emission tomography (PET) imaging (Máté et al., 2015). The *in vivo* imaging of tumor neo-angiogenesis using APN/CD13 specific NGR motif-based radiopharmaceuticals is an intensively researched area in the field of nuclear medicine and radiopharmacon development. The radiolabelling of NGR probes by diagnostic and therapeutic radionuclides (*e.g.*: ^{64}Cu (Li et al., 2014), ^{68}Ga (Máté et al., 2015; Satpati et al., 2017), ^{99m}Tc (Vats et al., 2017), ^{177}Lu (Vats et al., 2018), ^{188}Re (Ma et al., 2016)) provides an opportunity to monitor the *in vivo* biodistribution and tumor-targeting properties of the novel NGR derivatives, furthermore, give the possibility to follow the efficacy of anti-cancer therapies using *in vivo* molecular imaging. In addition, the detection of the APN/CD13 molecule is particularly important because it has been observed that it is not only a diagnostic but also a prognostic marker, that may predict the mortality and overall survival (Kessler et al., 2018; Schreiber et al., 2018).

In our previous studies we developed the ^{68}Ga-labelled NOTA-c(NGR) radipharmaceutical, which showed specific binding to APN/CD13 in chemically induced mesoblastic nephroma tumor model (Máté et al., 2015). Furthermore, in the last few years our research group synthesized novel cyclic NGR peptides containing thioether bond, and these new NGR-based probes were characterized under *in vitro* conditions (Enyedi et al., 2015, 2017). Based on our previous results, the aim of this present study was to labell our own developed cyclic NGR derivatives with ^{68}Ga radiometal, and evaluate and compare their APN/CD13 specificity *in vivo* by PET/MRI imaging using chemically induced hepatocellular carcinoma (He/De) and mesoblastic nephroma (Ne/De) tumor models.

2. Materials and Methods

2.1 Chemicals

The $^{68}Ge/^{68}Ga$-generator was obtained from Obninsk (Cyclotron Co., *Obninsk*, Russia). The reagents and solvents for peptide synthesis and purification were ordered from Reanal (Budapest, Hungary), IRIS Biotech GmbH (Marktredwitz, Germany) and Molar Chemicals Ltd (Budapest, Hungary). The chelators *p*-SCN-Bn-NOTA, NODAGA-NHS-ester and *p*-SCN-Bn-NODAGA were the products of Macrocyclics (Texas, USA) and CheMatech (Dijon, France). For radiolabelling experiment the chemicals were of Ultrapure® grade, so the HCl was produced from Merck KGaA (Darmstadt, Germany), moreover the water and acetate buffer from Sigma-Aldrich (St. Louis, Missouri, USA). All other chemicals were purchased from Sigma-Aldrich (St. Louis, Missouri, USA). The chemicals were of analytical grade and used without further purification.

2.2 Synthesis of linear precursor peptides

The linear precursor peptide derivatives were synthesised using standard solid-phase peptide synthesis with Fmoc/tBu strategy on Rink-Amide MBHA resin (0.5 g 0.64 mmol/g capacity) every case, then were purified with reverse-phase high performance liquid chromatography (RP-HPLC). The protocols were published earlier Máté et al. (2015) and Enyedi et al. (2015). Briefly, the synthesis were (i) DMF washing (4 × 0.5 min), (ii) Fmoc deprotection with 2% DBU, 2% piperidine in DMF (4 times; 2 + 2 + 5 + 10 min), (iii) DMF washing (10 x 0.5 min), (iv) coupling of Fmoc-protected amino acid derivative : DIC : HOBt in DMF (3 equiv each) (1 x 60 min), (v) DMF washing (3 x 0.5 min), (vi) DCM washing (2 x 0.5 min), (vii) ninhydrine assay. The crude linear peptides similarly to the cyclic peptides were purified on a KNAUER 2501 HPLC system (KNAUER, Bad Homburg, Germany) using a semi-preparative Phenomenex Luna C18 column (250 mm x 10 mm) with 10 μm silica (100 Å pore size) (Torrance, CA) with linear gradient elution (0 min 5 % B; 5 min 5 % B; 50 min 50 % B) and was engaged with an UV detector (set at 220 nm). The eluents were applied A (0.1% TFA in water) and B (0.1% TFA in MeCN-H_2O (80:20, v/v)) at a flow rate of 4 mL/min.

For the synthesis of cyclic NGR peptides with thioether linkage Glu was replaced by Cys in the sequence of KNGRE and the *N*-terminus was chloroacetylated with chloroacetic acid pentachlorophenyl ester (ClAc-OPcp) on the resin (Enyedi et al. (2015). In case of the

synthesis of the sarcosine-containing derivative *N*(Me)Gly was incorporated instead of Gly that can prevent the succinimide formation and rearrangement of NGR to *iso*DGR derivative.

2.3 Synthesis of cyclic NGR peptides

The synthesis of cyclic NGR peptides were described previously (Enyedi et al., 2015). The c[KNGRE]-NH_2 was prepared from semi-protected derivative using BOP coupling agent under the appropriate condition followed by the removal of ClZ protecting group from the side chain of Lys with anhydrous HF. The thioether bond was established in 0.1 M Tris buffer (pH=8.1). The linear precursor peptide was added to the solution in portions for 1 h. The final peptide concentration was 10 mg/mL in both cases. The reaction mixtures were stirred for further 2 h. The final products were purified (see above) and their purity and identity were analysed. Analytical RP-HPLC was accomplished on the same equipment using Phenomenex Luna C18 column (250 mm x 4.6 mm) with 5 μm silica (100 Å pore size) as a stationary phase with linear gradient elution (0 min 0% B; 5 min 0% B; 50 min 90% B) using the same eluents (above mentioned earlier). The flow rate was 1 mL/min. Peaks were detected at 214 nm. The purity of all compounds was over 95%. The pure products were characterized with ESI-MS by means an equipment of Esquire 3000+ ion trap mass spectrometer (Bruker Daltonics, Bremen, Germany).

2.4 Conjugation reaction of c[KNGRE]-NH_2 peptide with p-SCN-Bn-NOTA

The c[KNGRE]-NH_2 cyclic peptide was conjugated with macrocyclic bifunctional chelator *p*-SCN-Bn-NOTA. The thiourea bound was formed according to the procedure described by Máté et al. 2014. Briefly, 6.2 mg (12 μmol) from c[KNGRE]-NH_2 peptide was dissolved in 0.9 mL 0.1 M Na_2CO_3 buffer. 5.4 mg (9.6 μmol) of *p*-SCN-Bn-NOTA was solubilized in 100 μL DMSO and was introduced immediately to the c[KNGRE]-NH_2 peptide-solution. The reaction was stirred for 24 h at room temperature.

2.5 Conjugation reaction of c[KNGRE]-NH_2 peptide with NODAGA-NHS-ester

The c[KNGRE]-NH_2 cyclic peptide was conjugated with NODAGA-NHS-ester. 5 mg (8.6 μmol) from c[KNGRE]-NH_2 peptide was dissolved in 0.9 mL 0.1 M Na_2CO_3 buffer. 7.5 mg (10.2 μmol) of NODAGA-NHS-ester in 100 μL DMSO was introduced immediately to the peptide-solution. The reaction was stirred for 24 h at room temperature.

2.6 Conjugation reaction of c[CH_2-CO-Lys-Asn-Gly-Arg-Cys]-NH_2 peptide with *p*-SCN-Bn-NODAGA

5 mg (8 μmol) from c[CH_2-CO-Lys-Asn-Gly-Arg-Cys]-NH_2 peptide was dissolved in 0.9 mL 0.1 M Na_2CO_3 buffer. A freshly prepared solution of 4.6 mg (8.8 μmol) *p*-SCN-Bn-NODAGA in 100 μL DMSO was introduced, and the pH was adjusted to 8.4-8.5. The reaction mixture was shaken gently at room temperature, for 24 hours.

2.7 Conjugation reaction of c[CH_2-CO-Lys-Asn-*N*(Me)Gly-Arg-Cys]-NH_2) peptide with *p*-SCN-Bn-NODAGA

The c[CH_2-CO-Lys-Asn-*N*(Me)Gly-Arg-Cys]-NH_2) peptide analogue was functionalized a similar way, as earlier. 6 mg (9.3 μmol) from the c[CH_2-CO-Lys-Asn-*N*(Me)Gly-Arg-Cys]-NH_2) was introduced to the 0.9 mL 0.1 M Na_2CO_3 buffer, and it was mixed with the organic solution (100 μL DMSO) of the chelator (5.3 mg (10.2 μmol) p-SCN-Bn-NODAGA). After adjusting the pH 8.4-8.5 and mixing it at room temperature for overnight, the reaction was terminated.

2.8 Radiolabelling of peptides with $^{Ga}68$

For the radiolabelling experiments Obninsk-type (Cyclotron Co., *Obninsk*, Russia) $^{68}Ge/^{68}Ga$ generator was utilized. For yielding the radioactivity, a fractionated elution was applied, with 0.1 M, 5 mL aqueous HCl solution. The first 1.8 mL eluate was discarded, and the next 1-1.2 mL solution – this was the highest radioactive concentration of the nuclide – was collected. Exactly 1 mL from this stock was transferred to a 5 mL eppendorf tube, 160 μL of 1M NaOAc buffer was introduced, and finally the peptide-solution (3 mM, 5 μL) was mixed. This procedure resulted in a pH 4.0-4.1. Subsequently, the reaction was heated to 95°C for 5 minutes. The solution was let to cool down to room temperature, and the activity was immobilized on an OASIS® HLB 30 mg Cartridge, (Waters, Milford, Massachusetts, USA) preconditioned with ethanol and water (5:10 mL) according to the standard protocol. The column was rinsed with 2 mL of water and the activity was recovered with 0.5 mL of isotonic NaCl solution/EtOH 2:1 mixture. The product was passed through a sterile filter into a clean vial.

2.9 RP-HPLC methods

The chelator-conjugated, non-radioactive peptide analogues were purified by semi-preparative HPLC (KNAUER Wissenschaftliche Geräte GmbH, Berlin, Germany) equipped with an UV detector (column: Supelco Discovery® Bio Wide Pore C18, (150 mm x 10 mm), 10 μm particle size silica (Merck KGaA, Darmstadt, Germany). After a short isocratic period a linear gradient was applied (0 min 0% B; 4 min 0% B; 16 min 45% B). The eluent system was: A: 0.1% TFA in water and B: 0.1% TFA in MeCN-H_2O (95:5, v/v). 4.0 mL/min flow rate was applied and the UV detection was at 254 nm. The pure products were collected in a round-bottom flask and were lyophilized. The radiochemical purity of the radiolabelled peptides was assessed by RP-HPLC. (KNAUER HPLC). For the analytic HPLC experiments, a Supelco Discovery® Bio Wide Pore C18 column (250 mm x 4.6 mm) with 10 μm particle size silica (Merck KGaA, Darmstadt, Germany) was applied. The ulent program was the following: 0 min 0% B; 4 min 0% B; 14 min 40% B, (the eluents were detailed earlier). The flow rate was set to 1.2 mL/min. The peaks were detected with radio detector and UV detector (254 nm) paralel.

2.10 Determination of partition coefficient of ^{68}Ga-labelled ligands

Partition coefficient was calculated from the distribution rate of the radioactivity in 1-octanol and PBS solution. For the measurement, a small aliquot (10 μL) from the aqueous radioligand solution was introduced into a vial containing 0.49 mL of PBS and 0.5 mL of 1-octanol. To reach the equilibrium state, the solution was mixed firmly for 20 minutes and subsequently the phases were separated by means of a centrifugation for 5 minutes at 20.000 rpm. 3 times, 10 μL samples from each layer were introduced into the test tubes; and the radioactivity was determined with a gamma counter (Perkin-Elmer Packard Cobra, Waltham, MA, USA). The LogP value was calculated from the incomes of six parallel experiments.

2.11 Determination of *in vitro* stability of ^{68}Ga-labelled ligands

The chemical stability of ^{68}Ga-NODAGA-c(NGR) analogues were tested in PBS at 95ºC. 50 μL from the radioactive peptide solutions were diluted with 0.5 mL PBS. The solution was heated to 95ºC, and aliquots from the solution (25 μL) were directly injected to the reversed-phase HPLC at different time points (0, 30, 60, 90 and 120 min). For the determination of the radiochemical purity we used a gradient elution identical with the analytical program. For the determination of the enzymatic stability of the ^{68}Ga-NODAGA-c(NGR) analogues in serum, a

stock solution was prepared from 100 µL of the radioactive peptide solutions and 1 mL PBS. 20 µL from this solution was introduced to 480 µL of rat serum (purchased from Sigma-Aldrich, St. Louis, Missouri, USA) and the mixture was tempered at 37ºC. 50 µL of aliquots were taken from it at various time points (0, 30, 60, 90 and 120 min) and were mixed with equal volume of cold abs. EtOH. The precipitations were removed by centrifugation at 20.000 rpm for 5 min. The supernatants were saved and were diluted further with the starting eluent of the analytical HPLC. The conditions of the analysis were identical with the standard protocol. From the radiochemical purity the metabolic stability was calculated.

2.12 Experimental animals

16 weeks old, 250±20 g weighted male Fischer-344 rats (n=76; Animalab Ltd, Budapest, Hungary) were used for the experiments. Animals were housed under conventional conditions at 23±2°C with 50±10% humidity and artificial lighting with a circadian cycle of 12 h. The semi-synthetic diet (VRF1; Akronom Ltd., Budapest, Hungary) and drinking water were available *ad libitum* to all animals. The animal experiments were authorized by the Ethical Committee for Animal Research, University of Debrecen, Hungary (permission number: 8/2016/DEMÁB). Laboratory animals were kept and treated in compliance with all applicable sections of the Hungarian Laws and animal welfare directions and regulations of the European Union.

2.13 Subcutan tumor transplantation

Fischer-344 rats (n=64) were anaesthetized with 3% Isoflurane (Forane) using a small animal anaesthesia device (Eickemeyer, Tec3 Isoflurane Vaporizer), the left scapular region was depilated, disinfected and $5x10^6$ He/De (rat hepatocellular carcinoma; Trencsenyi et al., 2014) or Ne/De (rat mesoblastic nephroma, Máté et al., 2015) cells in 150 µL saline were injected subcutaneously.

2.14 *In vivo* PET imaging

Healthy control (n=3/radiopharmaceutical), He/De (n=5/radiopharmaceutical) and Ne/De (n=5/radiopharmaceutical) tumor-bearing F-344 rats were anaesthetized with 3% Forane using a dedicated small animal anaesthesia device and were injected with 12.3±1.2 MBq of ^{68}Ga-NOTA-c(NGR) or ^{68}Ga-NODAGA-c(NGR) or ^{68}Ga-NODAGA-c(NGR) (MG1) or ^{68}Ga-NODAGA-c(NGR) (MG2) in 150 µL saline via the lateral tail vein 11±1 after tumor cell inoculation. 90 min after radiotracer injection whole-body PET/MRI scans were peformed

using the preclinical *nanoScan* PET/MRI 1T device (Mediso LTD., Hungary). Special rat imaging chamber (MultiCell Imaging Chamber, Mediso LTD., Hungary) was used to eliminate the movement of rats and to maintain a permanent body temperature. For the anatomical localization of tissues and organs T1 weighted MRI scans (Material map) were performed. For the image reconstruction (3D-OSEM) and analysis of the PET images Nucline and InterView™ FUSION software (Mediso LTD., Hungary) were used, respectively. Standardized uptake value (SUV) was calculated using the following formula: SUV= [ROI activity (MBq/mL)]/[injected activity (MBq)/animal weight (g)].

2.15 *Ex vivo* biodistribution studies

After *in vivo* PET/MRI imaging, control and tumor-bearing rats were euthanized with 5% isoflurane. Three tissue samples were taken from selected tissues and organs and their weight and the radioactivities were measured with a calibrated gamma counter (Perkin-Elmer Packard Cobra, Waltham, MA, USA). The radiotracer uptake was expressed as %ID/g tissue.

2.16 Blocking experiments

For blocking experiments, He/De (n=3/radiopharmaceutical) and Ne/De (n=3/radiopharmaceutical) tumor-bearing rats were injected with 200 μg unlabelled c(NGR) in 100 μL saline via the lateral tail vein five minutes before the injection of ^{68}Ga-labelled NGR. After 90 minutes incubation time *in vivo* PET imaging and *ex vivo* studies were performed using the ^{68}Ga-labelled tracers, as described above.

2.17 Immunhistochemistry

For the demonstration of APN/CD13 expression, 4-5 μm thick sections of the formaldehyde fixed and paraffin embedded He/De and Ne/De tumors were exposed to the mouse anti-rat CD13 (Santa Cruz Biotechnology) at a dilution of 1:50 following deparaffination, rehydration and antigen retrieval (at pH 6.0). A HRP-labelled rabbit anti-mouse polymer antibody (Abcam, UK) and the Envision DAB detection kit (DAKO-Agilent Technologies, USA) were used for visualization of the specific antibody binding, followed by hematoxylin counterstaining. Photos were taken with Nikon Eclipse E800 (Nikon Corporation, Tokyo) microscope.

2.18 Statistical analysis

Experimental data was presented as mean±SD of at least three independent experiments. The significance was calculated by Student's t-test (two-tailed), two-way ANOVA and Mann-Whitney U-test. The significance level was set at $p \leq 0.05$ unless otherwise indicated.

3. Results

3.1 Chemistry and radiochemistry

The linear peptides were synthesized by a solid phase method on a Rink-Amide MBHA resin (0.5 g 0.64 mmol/g capacity) every case. The peptides were cyclized successfully. The purity of cyclized peptides was found to be 95%≤ with analytical HPLC. The pure chelator-conjugated peptide analogues were characterized by mass spectrometry (ESI-MS: Shimadzu LCMS IT-TOF Mass Spectrometer, Shimadzu Corp., Tokyo, Japan): measured: m/z 941.48 for [M+H]+; calculated 941.74 of NODAGA-c(NGR), m/z 1137.63 for [M+H]+; calculated 1137.31 of c[CH_2-CO-Lys(NODAGA)-Asn-Gly-Arg-Cys]-NH_2 = (NODAGA-c(NGR) (MG1)) and measured: m/z 1151.63 for [M+H]+; calculated 1151.31 of c[CH_2-CO-Lys(NODAGA)-Asn-N(Me)Gly-Arg-Cys]-NH_2 = (NODAGA-c(NGR) (MG2)). ^{68}Ga labelling procedures were accomplished within 15-20 min. The radiochemical purity was >99% after formulation all cases. The molar activity of radiopharmaceuticals was found to be 5.49-7.36 GBq/μmol. The chemical structures and synthesis of chelator peptide-conjugates and radiolabelling of analogues are shown in Fig. 1. and in Supplementary material Figures 1-4.

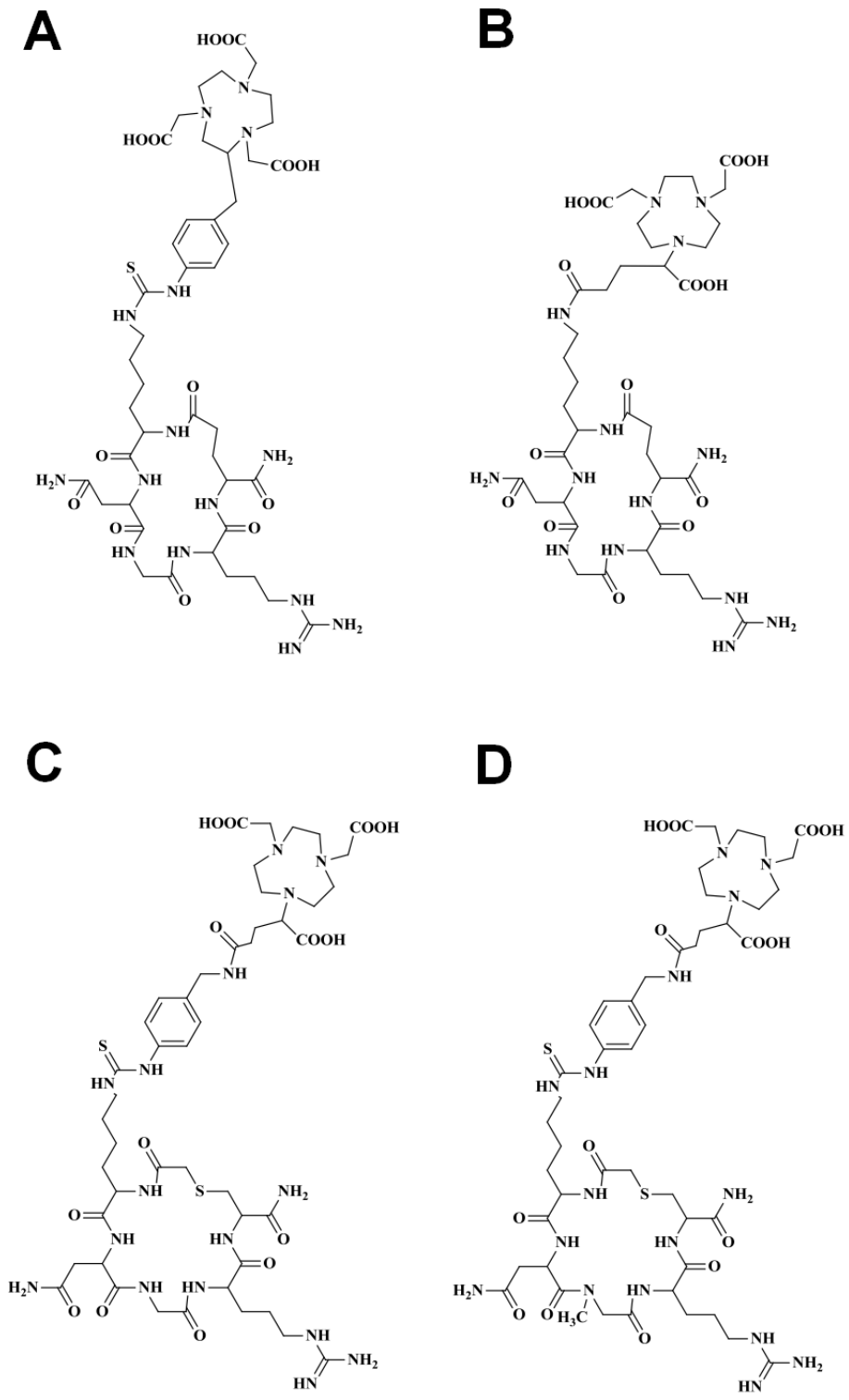

Fig. 1. Chemical structures of NOTA-c(NGR) (A), NODAGA-c(NGR) (B), c[CH_2-CO-Lys(NODAGA)-Asn-Gly-Arg-Cys]-NH_2 (NODAGA-c(NGR) (MG1)) (C), c[CH_2-CO-Lys(NODAGA)-Asn-*N*(Me)Gly-Arg-Cys]-NH_2 (NODAGA-c(NGR) (MG2)) (D).

3.2 Partition coefficient and *in vitro* stability of ^{68}Ga-labelled c(NGR) derivatives

The partition coefficient (LogP) of ^{68}Ga-NODAGA-c(NGR) was measured to be –4.07±0.13 and ^{68}Ga-NODAGA-c(NGR) (MG1) determined to be –2.33±0.14, while the *N*-methyl-glycine containing analogue, ^{68}Ga-NODAGA-c(NGR) (MG2) proved to be –2.29±0.13, suggesting that all of the radiotracers are hydrophilic. Incubation of ^{68}Ga-NODAGA-c(NGR) in rat serum (*in vitro* stability) for 120 min did not result in any additional peak or change in radioHPLC retention times/pattern: 98.90%, 98.11%, 97.90, 97.76%, 97.64%. The methyl substitution resulted in bigger effect on their chemical stability. During the measurement on elevated temperature (PBS; pH=7.4; T=95ºC) both analogues proved to be stable, only after 120 minutes we were able to detect significant difference in stability, but the ratios of the intact molecules were above 95%. The decomposition of the original structure was definitely more articular in the presence of a rat serum. The radiochemical purity of the different time points was 100%, 86.75%, 73.4%, 61.11%, 55.42% in the case of ^{68}Ga-NODAGA-c(NGR) (MG1), while 100%, 92.45%, 84.47%, 78.32%, and 75.42% for ^{68}Ga-NODAGA-c(NGR) (MG2), respectively. These results suggest a moderate stability of these compounds in the blood, but clearly indicate the positive effect of the *N*-methylation avoiding the Asn deamidation.

3.3 *In vivo* PET/MRI and *ex vivo* biodistribution studies in control rats

For the determination of the normal biodistribution of ^{68}Ga-NOTA-c(NGR), ^{68}Ga-NODAGA-c(NGR), ^{68}Ga-NODAGA-c(NGR) (MG1), and ^{68}Ga-NODAGA-c(NGR) (MG2) whole-body PET/MRI imaging and *ex vivo* tissue distribution studies were performed 90 min after intravenous injection of the radiotracers using healthy control F-344 rats. Representative decay-corrected coronal PET/MRI images of healthy rats are shown in Fig. 2. After the qualitative analysis of the PET images we found low radiotracer accumulation in the abdominal and thoracic organs using the four radiotracers after 90 min incubation time. In contrast, the urinary system (bladder with urine) was clearly visualized (Fig. 2 white arrows).
By the quantitative SUV analysis of the PET images (Fig. 2E) no significant differences (at $p \leq 0.05$) were found between the SUVmean values of the investigated organs and tissues when the accumulation of ^{68}Ga-NOTA-c(NGR), ^{68}Ga-NODAGA-c(NGR), ^{68}Ga-NODAGA-c(NGR) (MG1) and ^{68}Ga-NODAGA-c(NGR) (MG2) were compared.

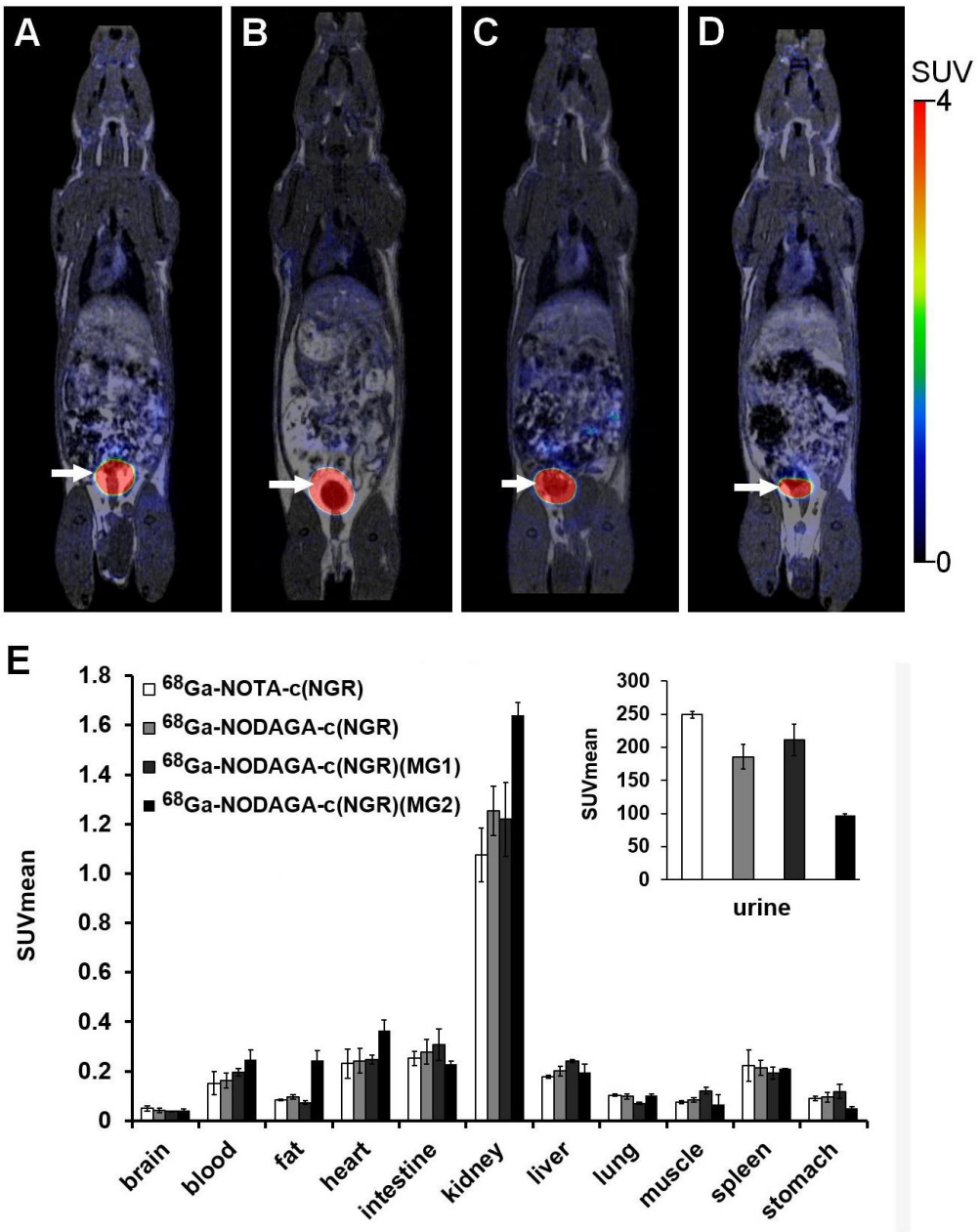

Fig. 2. *In vivo* PET/MRI assessment of ^{68}Ga-NOTA-c(NGR) (A), ^{68}Ga-NODAGA-c(NGR) (B), ^{68}Ga-NODAGA-c(NGR) (MG1) (C), and ^{68}Ga-NODAGA-c(NGR) (MG2) (D) accumulation in healthy control F-344 rats. Representative decay-corrected coronal PET/MRI images were obtained 90 min after intravenous injection of the radiotracers. White arrows: bladder (urine). E: quantitative SUV analysis of tracer uptake in control animals

(n=3/radiopharmaceutical) 90 min post-injection. SUV: standardized uptake value. SUV values are presented as mean±SD.

These *in vivo* PET/MRI results correlated well with the *ex vivo* data shown in Fig. 3. For *ex vivo* distribution studies rats were sacrificed after PET/MRI imaging and after autopsy the accumulated radioactivity of the tissues were assessed by gamma counter. Remarkable radiotracer accumulation was observed in kidneys (approx. %ID/g: 0.5) and urine (approx. %ID/g: 50-85), and slight radiotracer uptake was observed with low %ID/g values in other organs and tissues. By comparing the amount (%ID/g) of radiopharmaceuticals in the selected organs, we found that the ^{68}Ga-NODAGA-c(NGR) (MG2) showed a relatively higher accumulation in the blood, liver and spleen, however, this difference was not significant.

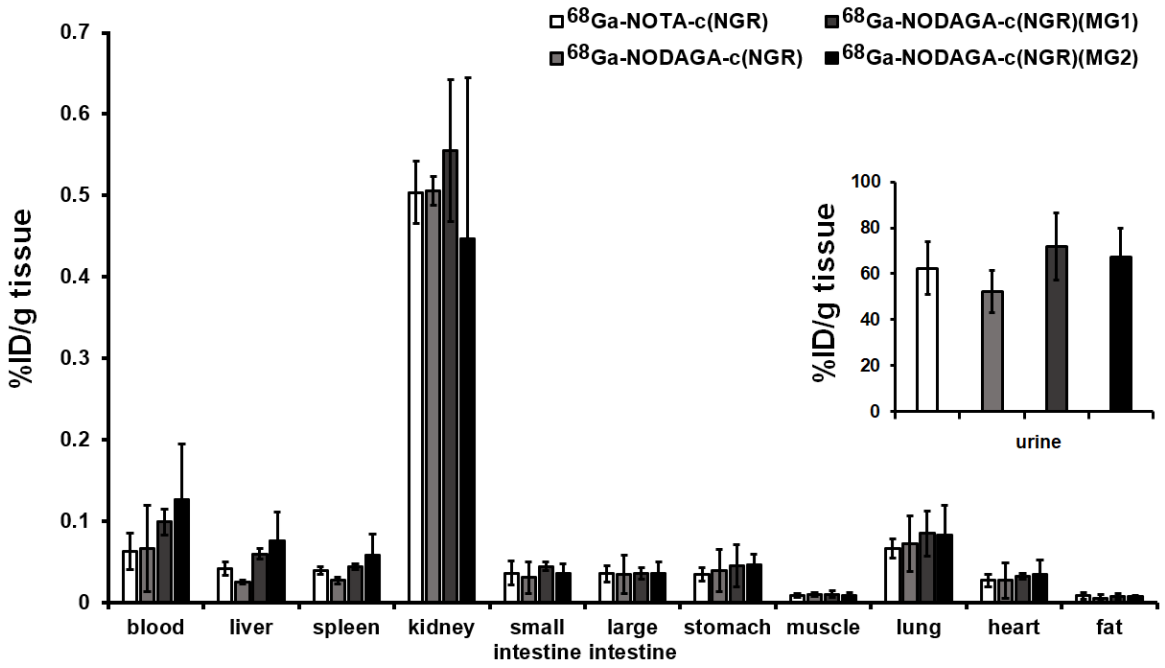

Fig. 3. *Ex vivo* biodistribution of ^{68}Ga-labelled NGR derivatives in healthy control F-344 rats 90 min after intravenous injection of the radiotracers. %ID/g values are presented as mean±SD.

3.4 *In vivo* PET/MRI imaging and *ex vivo* studies of He/De and Ne/De tumor-bearing rats

For the *in vivo* assessment of the APN/CD13 specificity of the ^{68}Ga-labelled cNGR-based tracers He/De (hepatocellular carcinoma) and Ne/De (mesoblastic nephroma) tumor-bearing rats were injected intravenously with ^{68}Ga-NOTA-c(NGR), ^{68}Ga-NODAGA-c(NGR), ^{68}Ga-NODAGA-c(NGR) (MG1) or ^{68}Ga-NODAGA-c(NGR) (MG2) and after 90 min incubation time whole-body PET/MRI scans were acquired. Representative whole-body decay-corrected coronal and axial PET/MRI images of He/De and Ne/De tumors are shown in Fig. 4 and 5., respectively. The subcutaneously growing tumors were clearly visualized using ^{68}Ga-NOTA-c(NGR), ^{68}Ga-NODAGA-c(NGR) and ^{68}Ga-NODAGA-c(NGR) (MG1) 90 min after the tracer injection, however, ^{68}Ga-NODAGA-c(NGR) (MG2) radiopharmaceutical showed the lowest accumulation in both tumors (Fig. 4 and 5, white arrows). This observation was confirmed by the quantitative SUV analysis (Fig. 4E and 5E), where we found significantly ($p\leq0.05$ and $p\leq0.01$) lower uptake in He/De (SUVmean: 0.11±0.03; SUVmax: 0.63±0.26) and Ne/De (SUVmean: 0.29±0.03; SUVmax: 1.13±0.07) tumors using ^{68}Ga-NODAGA-c(NGR) (MG2) than that of the SUV values of the three other radiotracers, where the SUVmean and SUVmax data were approximately 2-5-fold higher in He/De tumors and approximately 1.5-3-fold higher in Ne/De tumors. A similar trend was observed in the quantitative SUV analysis of tumor-to-background (muscle) ratios in both investigated tumors, where the ^{68}Ga-NODAGA-c(NGR) (MG2) radiotracer showed the lowest accumulation. Overall, it was found that NOTA- and NODAGA-conjugated c(NGR) molecules showed higher accumulation in He/De and Ne/De tumors than the NODAGA conjugated MG1 and MG2 probes (Supplementary material Table 1 and 2).

For the investigation of APN/CD13 specificity of ^{68}Ga-NOTA-c(NGR), ^{68}Ga-NODAGA-c(NGR), ^{68}Ga-NODAGA-c(NGR) (MG1) or ^{68}Ga-NODAGA-c(NGR) (MG2) *in vivo* blocking studies were performed at 90 min post injection in the presence of approx. 200 μg unlabelled c(NGR). Fig. 4 and 5 (lower rows of A-D panels) shows that the pre-injection of the unlabelled c(NGR) reduced the accumulation of the four investigated radiotracers in He/De and Ne/De tumors. The quantitative SUV analysis (Fig. 4F, 5F and Supplementary material Table 1 and Table 2) confirmed this observation, and the uptake of the radiotracers of He/De and Ne/De significantly decreased in the presence of unlabelled c(NGR), confirming the CD13 binding specificity *in vivo*.

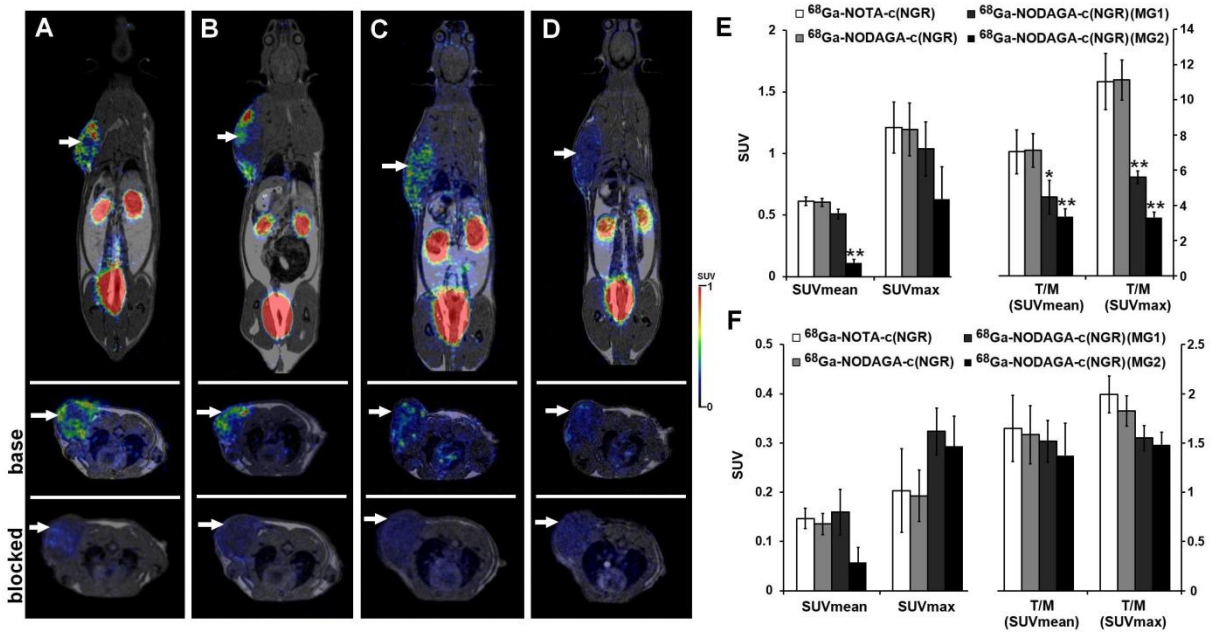

Fig. 4. *In vivo* assessment of ^{68}Ga-labelled NGR derivatives uptake of He/De tumors. Representative coronal (upper row) and transaxial (middle row: base; lower row: blocked (*see 2.16. Materials and methods*)) PET/MRI images of tumor-bearing rats 90 min after intravenous injection of ^{68}Ga-NOTA-c(NGR) (A), ^{68}Ga-NODAGA-c(NGR) (B), ^{68}Ga-NODAGA-c(NGR) (MG1) (C), and ^{68}Ga-NODAGA-c(NGR) (MG2) (D). Quantitative SUV analysis of base (E) and blocked (F) radiotracer uptake data in Ne/De tumors 90 min post inj. and 11±1 days after subcutaneous injection of He/De tumor cells. Significance level: $p \leq 0.05$ (*) and $p \leq 0.01$ (**). SUV: standardized uptake value; T/M: tumor-to-muscle ratio. SUV values are presented as mean±SD.

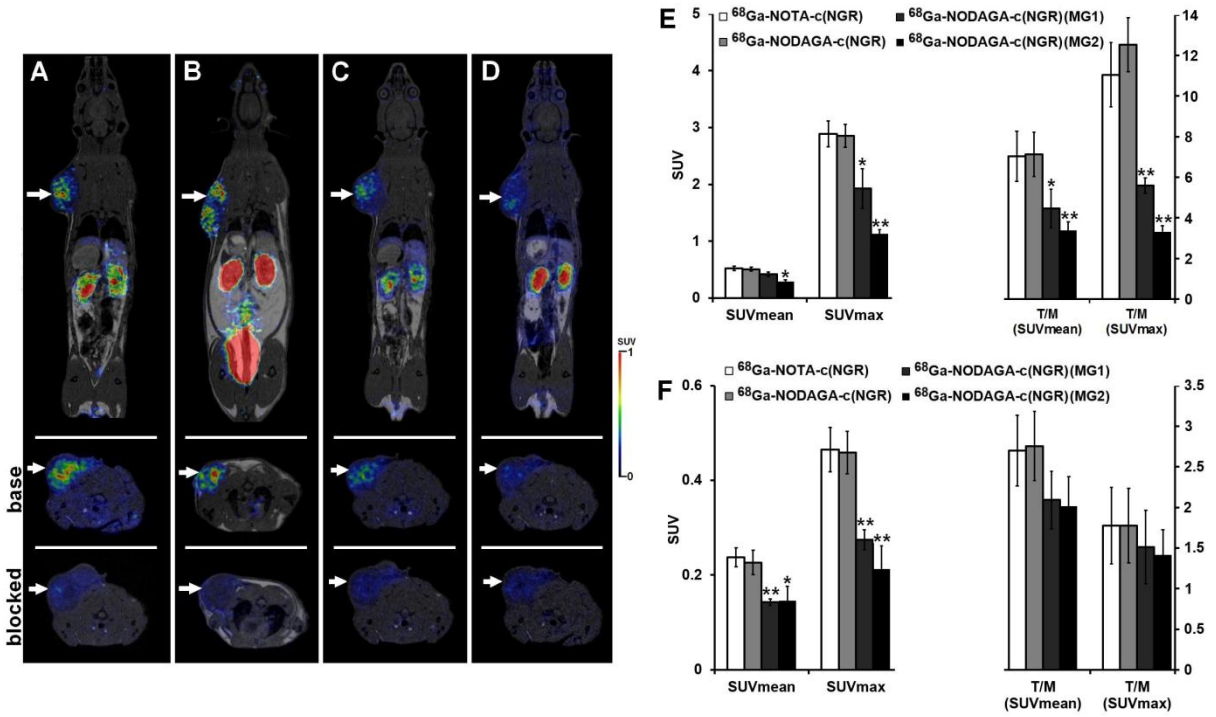

Fig. 5. *In vivo* assessment of ^{68}Ga-labelled NGR derivatives uptake of Ne/De tumors. Representative coronal (upper row) and transaxial (middle row: base; lower row: blocked (*see 2.16. Materials and methods*)) PET/MRI images of tumor-bearing rats 90 min after intravenous injection of ^{68}Ga-NOTA-c(NGR) (A), ^{68}Ga-NODAGA-c(NGR) (B), ^{68}Ga-NODAGA-c(NGR) (MG1) (C), and ^{68}Ga-NODAGA-c(NGR) (MG2) (D). Quantitative SUV analysis of base (E) and blocked (F) radiotracer uptake data in Ne/De tumors 90 min post inj. and 11±1 days after subcutaneous injection of Ne/De tumor cells. Significance level: $p \leq 0.05$ (*) and $p \leq 0.01$ (**). SUV: standardized uptake value; T/M: tumor-to-muscle ratio. SUV values are presented as mean±SD.

Similarly to the *in vivo* SUV data, the *ex vivo* %ID/g (Table 1) data represent that the ^{68}Ga-NOTA-c(NGR) showed the highest accumulation in the investigated tumors, followed by the ^{68}Ga-NODAGA-c(NGR), ^{68}Ga-NODAGA-c(NGR) (MG1), and finally the ^{68}Ga-NODAGA-c(NGR) (MG2). The success of blocking was also confirmed by *ex vivo* data, where significantly ($p \leq 0.01$) lower radiotracer accumulation was found in the blocked tumors than that of the non-blocked 90 min post injection. By using the four investigated c(NGR)-based radiotracers, no significant differences were found between He/De and Ne/De tumors by either *in vivo* imaging or *ex vivo* biodistribution measurements.

Table 1

Ex vivo assessment of the accumulation of the four ^{68}Ga-labelled c(NGR) derivatives in experimental subcutaneous He/De and Ne/De tumors 90 min after tracer injection and 11±1 days after tumor cell inoculation. %ID/g tissue values are presented as mean±SD. Significance level between blocked and non-blocked tumors at 90 min: $p \leq 0.01$ (**). 200 μg unlabelled c(NGR) was used for blocking. T/M: tumor-to-muscle ratio.

Tumor	^{68}Ga-NOTA-c(NGR)	^{68}Ga-NODAGA-c(NGR)	^{68}Ga-NODAGA-c(NGR)(MG1)	^{68}Ga-NODAGA-c(NGR)(MG2)
He/De (n=5)	0.69 ± 0.11	0.65 ± 0.06	0.45 ± 0.11	0.34 ± 0.08
He/De T/M ratio	9.99 ± 1.60	7.95 ± 1.39	6.13 ± 0.96	5.56 ± 0.94
He/De (blocked) (n=3)	0.12 ± 0.04**	0.09 ± 0.02**	0.14 ± 0.01**	0.11 ± 0.02**
Ne/De (n=5)	0.83 ± 0.23	0.79 ± 0.18	0.66 ± 0.12	0.40 ± 0.08
Ne/De T/M ratio	7.10 ± 1.27	6.58 ± 1.24	6.15 ± 0.77	5.73 ± 0.41
Ne/De blocked (n=3)	0.10 ± 0.02**	0.11 ± 0.04**	0.17 ± 0.05**	0.09 ± 0.03**

3.5 Immunohistochemistry

The expression of APN/CD13 was verified by immunostaining of subcutaneously growing He/De and Ne/De tumors. Figure 6 shows the strong but scattered APN/CD13 positivity (brown staining) throughout the masses of the tumor, which correlated well with the heterogenous radiotracer uptake seen in the *in vivo* PET images, further confirming the strong binding affinity of ^{68}Ga-labelled c(NGR) probes to the APN/CD13 molecule.

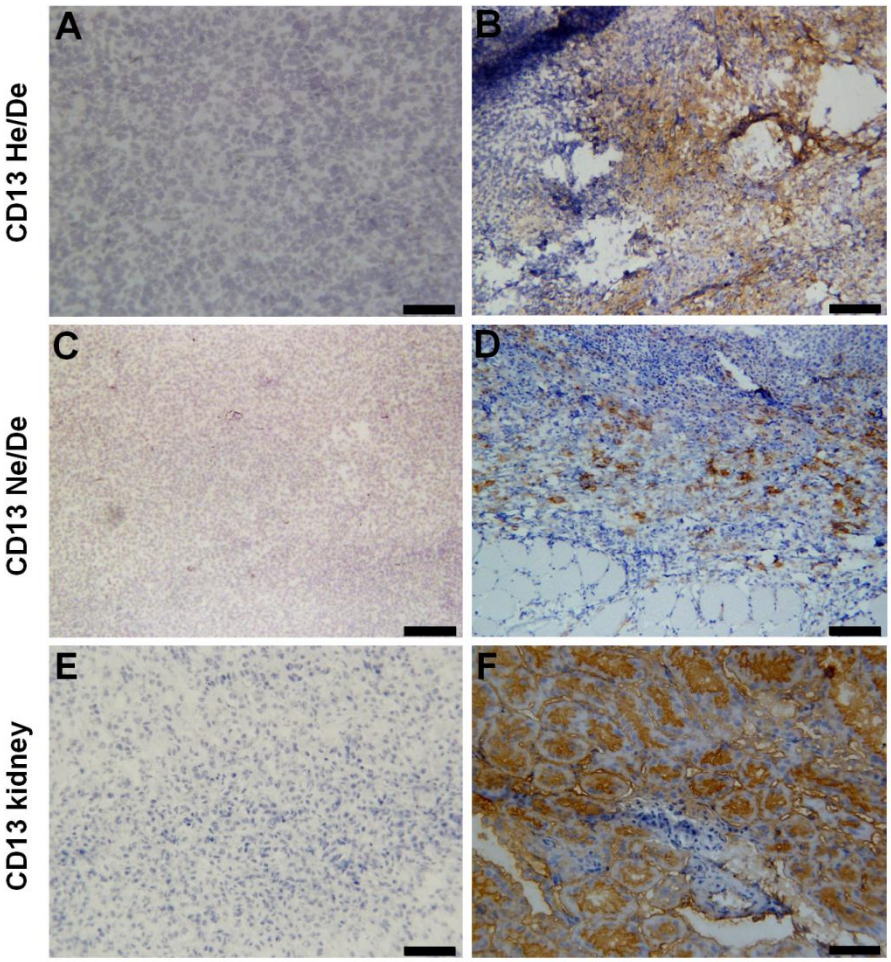

Fig. 6. Immunohistological analysis of APN/CD13 expression in subcutaneously growing He/De (B) and Ne/De (D) tumors 11 days after tumor cell inoculation. Rat kidney (F) was used as positive control for APN/CD13. Anti-CD13 primary antibody was visualized with 3,3-diaminobenzidine (DAB) (brown staining). For negative control (A, C, E) DAB was used in the absence of the primary antibody. Magnification: 20X. Bar: 200 μm.

4. Discussion

In vivo imaging of tumor neo-angiogenesis is an intensively researched area in clinical and preclinical positron emission tomography and in the development of radiopharmaceuticals. Confirming the presence of neo-angiogenic markers in tumors by *in vivo* PET imaging using specific radiopharmaceuticals can greatly assist the detection of tumors at an early stage, just after the angiogenic switch, and the selection and follow-up of the appropriate anticancer therapy. In the human clinical routine PET imaging ^{18}FDG is the most commonly used radiopharmaceutical for the detection of tumors, metastases and for monitoring the efficacy of anticancer therapies (De Ruysscher et al., 2016). However, ^{18}FDG is not specific for angiogenic molecules; furthermore, it is known that ^{18}F-FDG has low accumulation and poor diagnostic efficiency in *e.g.* well-differentiated hepatocellular carcinoma tumors (Gao et al., 2017). Due to the above facts, there is a growing demand for the development of specific radiopharmaceuticals in the molecular imaging of tumor associated neo-angiogenesis.

In this present study subcutaneously transplanted chemically induced syngeneic hepatocellular carcinoma (He/De) and mesoblastic nephroma (Ne/De) rat models were used for the *in vivo* assessment of APN/CD13 specificity of our newly synthesized and ^{68}Ga-labelled NGR derivatives by *in vivo* PET/MRI imaging. It is known from the literature, that the asparaginyl–glycinyl–arginine (NGR) peptide is a specific ligand of APN/CD13, furthermore, several studies have reported that the radiolabelled NGR peptide with positron emitting (*e.g.*: ^{64}Cu, ^{68}Ga) isotopes served useful radiotracers for the *in vivo* imaging of APN/CD13 receptor expression of tumors and neovasculature (Máté et al., 2015; Shao et al., 2014a, 2014b; Zhang et al., 2014). For the evaluation of the chemical or metabolic stability on the image quality we have tested different parameters. In the case of the c[KNGRE]-NH_2 – where the targeting moiety owes an extraordinarly good chemical inertness – the replacement of the chelator subunite was performed. The new analogue – NODAGA-c(NGR) – has practically every subunit identical with the "reference compound" (NOTA-c(NGR)), except the lack of aromatic ring, and the difference in the bond of the conjugation. Therefore, we hypothetised a very similar behavior, but fine tuned with the hydrophile/lipophile balance. On the other hand, Corti and coworkers (Corti et al., 2017) has published that glycine *N*-methylation in the NGR-sequence can completely prevents asparagine deamidation without impairing CD13 recognition. This finding promotes us to validate the use of *N*-Me-Gly in the five amino acid composed ring. To visualizate the effect of the exchange we have to select a

more unstable NGR-analogue, namely a thioether cyclized NGR analogue c[CH_2-CO-Lys-Asn-Gly-Arg-Cys]-NH_2, due to 40% of this substance has decomposed in PBS (pH = 7.4) after 24 hours (Enyedi et al., 2015). The MG1 and MG2 analogues were conjugated with the identical methodology, like the lead-compound, but with a NODAGA – type chelator, resulting in thiourea linkage and an extra aromatic ring, to maintain the comparable hydrophilic behavior of this part of the molecule to NOTA-c(NGR).

The *in vitro* lipophilicity experiments demonstrated that newly synthesized ^{68}Ga-NODAGA-c(NGR) derivatives are highly hydrophilic (log*P* values were between approximately - 2.2 and - 4.1), and this observation was confirmed by *in vivo* PET imaging and *ex vivo* biodistribution studies performed on healthy control F-344 rats. These biodistribution studies revealed that ^{68}Ga-labelled c(NGR) derivatives were mainly excreted through the urinary system, due to their hydrophilic properties, furthermore, the abdominal (except for the kidneys) and thoracic organs showed very low radiotracer uptake after 90 min incubation time (Fig. 2). The relatively higher liver spleen and lung uptake of ^{68}Ga-NODAGA-c(NGR) (MG2) may be attributed to its lower hydrophilicity. This low accumulation of the c(NGR)-based radiotracers in the abdominal organs correlated well with other studies, where the biodistribution of ^{68}Ga-DOTA-NGR (Zhang et al., 2014), ^{68}Ga-NODAGA-NGR (Satpati et al., 2018) and ^{68}Ga-NOTA-NGR (Shao et al., 2014a, 2014b) molecules were investigated. Furthermore, the low radiotracer accumulation in healthy tissues also allowed for high quality images with low background activity (high T/M ratios) to be obtained. This property greatly facilitates image evaluation and tumor identification when preparing the diagnostic report. However, it is important to note that, in addition to NGR molecules with different structures, the physicochemical properties of the chelator (*e.g.*: HBED-CC, NOTA, NODAGA) used greatly influence the accumulation of radiopharmaceuticals in the examined organs (Satpati et al., 2018, Trencsenyi et al., 2017).

In this paper, for the *in vivo* and *ex vivo* assessment of the APN/CD13 targeting properties of our ^{68}Ga-labelled c(NGR)-based tracers He/De (hepatocellular carcinoma) and Ne/De (mesoblastic nephroma) tumor-bearing rats were injected intravenously with ^{68}Ga-NOTA-c(NGR), ^{68}Ga-NODAGA-c(NGR), ^{68}Ga-NODAGA-c(NGR) (MG1) or ^{68}Ga-NODAGA-c(NGR) (MG2) and 90 min post injection whole-body PET/MRI scans, then organ distribution studies were performed (Fig. 4, 5 and Table 1). Although He/De and Ne/De tumors were well identifiable using all the four radiopharmaceuticals, different accumulation was observed in the investigated tumors. Overall, it was found that NOTA- and NODAGA-conjugated c(NGR) molecules showed higher accumulation in He/De and Ne/De tumors than

the NODAGA conjugated MG1 and MG2 probes (Supplementary material Table 1 and 2). This difference between the four APN/CD13 probes can be due to the chemical properties described above (lower stability of MG1 and probably the lower binding efficiency of *N*-methylated version), furthermore, - as a limitation - it is important to note that although studies have been performed at the same tumor size, it is known that the expression of angiogenic markers changes with tumor growth, can be influenced by tumor type, and is highly dependent on the presence and degree of hypoxia (Deshpande et al., 2011).

In our *in vivo* and *ex vivo* blocking experiments using the unlabelled c(NGR), the accumulation of the investigated radiotracers in both tumors reduced significantly ($p \leq 0.01$) (Fig. 4, 5 and Table 1), similarly, to previous studies with other ^{68}Ga-labelled NGR-conjugates, where human xenograft tumors (Satpati et al., 2018; Shao et al., 2014a, 2014b; Zhang et al., 2014) were investigated. These blocking results suggest that our ^{68}Ga-labelled c(NGR) derivatives specifically bind to the APN/CD13 receptors. Earlier (Máté et al., 2015), the presence of APN/CD13 expression of Ne/De tumors was verified by western blot analysis, and in this work the expression was confirmed on He/De and Ne/De tumors by immunohistochemistry (Fig. 6).

5. Conclusion

Among markers of tumor neo-angiogenesis, APN/CD13 is a very promising target in positron emission tomography imaging, however, the selection of the appropriate ^{68}Ga-labelled NGR-based radiopharmaceutical (*e.g.*: ^{68}Ga-NOTA- and NODAGA-c(NGR) with the highest binding affinity in this study) is critical for the precise detection of tumors neo-angiogenesis and for monitoring the efficacy of anticancer therapy.

Declaration of Competing Interest

The authors declare that they have no known competing financial interests or personal relationships that could have appeared to influence the work reported in this paper.

Acknowledgements

This work was supported by a Bolyai fellowship to GT. Furthermore, by the Thematic Excellence Programme of the Ministry for Innovation and Technology in Hungary (ED_18-1-2019-0028), within the framework of the Space Sciences thematic programme of the University of Debrecen. This research was also supported by the National Research, Development and Innovation Office under grant NKFIH K119552 and NVKP_16-1-2016-0036, and by EFOP-3.6.3-VEKOP-16-2017-00009 co-financed by EU and the European Social Found. As a sign of our respect, in the name of the molecules "MG" means Professor Gábor Mező, who is the main developer of the cNGR peptides.

References

Buehler, A., van Zandvoort, M.A., Stelt, B.J., Hackeng, T.M., Schrans-Stassen, B.H., Bennaghmouch, A., Hofstra, L., Cleutjens, J.P., Duijvestijn, A., Smeets, M.B., de Kleijn, D.P., Post, M.J., de Muinck, E.D., 2006. cNGR, a novel homing sequence for CD13/APN targeted molecular imaging of murine cardiac angiogenesis in vivo. Arterioscler. Thromb. Vasc. Biol. 26, 2681−2687. https://doi.org/10.1161/01.ATV.0000245807.65714.0b.

Carmeliet, P., Jain, R.K., 2000. Angiogenesis in cancer and other diseases. Nature. 407, 249–257. https://doi.org/10.1038/35025220.

Chen, K., Ma, W., Li, G., Wang, J., Yang, W., Yap, L.P., Hughes, L.D., Park, R., Conti, P.S., 2013. Synthesis and evaluation of 64Cu-labeled monomeric and dimeric NGR peptides for MicroPET imaging of CD13 receptor expression. Mol. Pharm. 10, 417−427. https://doi.org/10.1021/mp3005676.

Colombo, G., Curnis, F., De Mori, G.M., Gasparri, A., Longoni, C., Sacchi, A., Longhi, R., Corti, A., 2002. Structure-activity relationships of linear and cyclic peptides containing the NGR tumor-homing motif. J. Biol. Chem. 277, 47891–47897. https://doi.org/10.1074/jbc.M207500200.

Corti, A., Curnis, F., Arap, W., Pasqualini, R., 2008. The neovasculature homing motif NGR, more than meets the eye. Blood. 112, 2628−2635. https://doi.org/10.1182/blood-2008-04-150862.

Corti, A., Gasparri, A.M., Ghitti, M., Sacchi, A., Sudati, F., Fiocchi, M., Buttiglione, V., Perani, L., Gori, A., Valtorta, S., Moresco, R.M., Pastorino, F., Ponzoni, M., Musco, G., Curnis, F., 2017. Glycine *N*-methylation in NGR-Tagged Nanocarriers Prevents Isoaspartate formation and Integrin Binding without Impairing CD13 Recognition and Tumor Homing. Adv. funct. mat. 27, 1701245. https://doi.org/10.1002/adfm.201701245.

De Ruysscher, D., Haustermans, K., Thorwarth, D., 2016. FDG and Beyond. Recent Results Cancer Res. 198, 163-173. https://doi.org/10.1007/978-3-662-49651-0_8.

Deshpande, N., Ren, Y., Foygel, K., Rosenberg, J., Willmann, J.K., 2011. Tumor angiogenic marker expression levels during tumor growth: longitudinal assessment with molecularly targeted microbubbles and US imaging. Radiology. 258, 804-811. https://doi.org/10.1148/radiol.10101079.

Enyedi, K.N., Czajlik, A., Knapp, K., Láng, A., Majer, Z., Lajkó, E., Kőhidai, L., Perczel, A., Mező, G., 2015. Development of cyclic NGR peptides with thioether linkage: structure and dynamics determining deamidation and bioactivity. J. Med. Chem. 58, 1806-1817. https://doi.org/10.1021/jm501630j.

Enyedi, K.N., Tóth, S., Szakács, G., Mező, G., 2017. NGR-peptide-drug conjugates with dual targeting properties. PLoS ONE. 12, e0178632. https://doi.org/10.1371/journal.pone.0178632.

Folkman, J., 2002. Role of angiogenesis in tumor growth and metastasis. Semin. Oncol. 29, 15–18. https://doi.org/10.1053/sonc.2002.37263.

Gao, Y., Wang, Z., Ma, X., Ma, W., Zhao, M., Fu, T., Li, G., Wang, S., Wang, Z., Yang, W., Kang, F., Wang, J., 2017. The uptake exploration of 68Ga-labeled NGR in well-differentiated hepatocellular carcinoma xenografts: Indication for the new clinical translational of a tracer based on NGR. Oncol. Rep. 38, 2859-2866. https://doi.org/10.3892/or.2017.5933.

van Hensbergen, Y., Broxterman, H.J., Rana, S., van Diest, P.J., Duyndam, M.C., Hoekman, K., Pinedo, H.M., Boven, E., 2004. Reduced growth, increased vascular area, and reduced response to cisplatin in CD13-overexpressing human ovarian cancer xenografts. Clin. Cancer Res. 10, 1180−1191. https://doi.org/10.1158/1078-0432.ccr-0482-3.

Higuchi, T., Bengel, F.M., Seidl, S., Watzlowik, P., Kessler, H., Hegenloh, R., Reder, S., Nekolla, S.G., Wester, H.J., Schwaiger, M., 2008. Assessment of alphavbeta3 integrin

expression after myocardial infarction by positron emission tomography. Cardiovasc. Res. 78, 395−403. https://doi.org/10.1093/cvr/cvn033.

Jászai, J., Schmidt, M.H.H., 2019. Trends and Challenges in Tumor Anti-Angiogenic Therapies. Cells. 8, 1102. https://doi.org/10.3390/cells8091102.

Kessler, T., Baumeier, A., Brand, C., Grau, M., Angenendt, L., Harrach, S., Stalmann, U., Schmidt, L.H., Gosheger, G., Hardes, J., Andreou, D., Dreischalück, J., Lenz, G., Wardelmann, E., Mesters, R.M., Schwöppe, C., Berdel, W.E., Hartmann, W., Schliemann, C., 2018. Aminopeptidase N (CD13): Expression, Prognostic Impact, and Use as Therapeutic Target for Tissue Factor Induced Tumor Vascular Infarction in Soft Tissue Sarcoma. Transl. Oncol. 11, 1271-1282. https://doi.org/10.1016/j.tranon.2018.08.004.

Li, G., Wang, X., Zong, S., Wang, J., Conti, P.S., Chen, K., 2014. MicroPET imaging of CD13 expression using a (64)Cu-labeled dimeric NGR peptide based on sarcophagine cage. Mol. Pharm. 11, 3938-3946. https://doi.org/10.1021/mp500354x.

Ma, W., Shao, Y., Yang, W., Li, G., Zhang, Y., Zhang, M., Zuo, C., Chen, K., Wang, J., 2016. Evaluation of (188)Re-labeled NGR-VEGI protein for radioimaging and radiotherapy in mice bearing human fibrosarcoma HT-1080 xenografts. Tumour Biol. 37, 9121-9129. https://doi.org/10.1007/s13277-016-4810-y.

Máté, G., Kertész, I., Enyedi, K.N., Mező, G., Angyal, J., Vasas, N., Kis, A., Szabó, É., Emri, M., Bíró, T., Galuska, L., Trencsényi, G., 2015. In vivo imaging of Aminopeptidase N (CD13) receptors in experimental renal tumors using the novel radiotracer (68)Ga-NOTA-c(NGR). Eur. J. Pharm. Sci. 69, 61–71. https://doi.org/10.1016/j.ejps.2015.01.002.

Negussie, A.H., Miller, J.L., Reddy, G., Drake, S.K., Wood, B.J., Dreher, M.R., 2010. Synthesis and in vitro evaluation of cyclic NGR peptide targeted thermally sensitive liposome. J. Control Release. 143, 265–273. https://doi.org/10.1016/j.jconrel.2009.12.031.

Otsuki, T., Nakashima, T., Hamada, H., Takayama, Y., Akita, S., Masuda, T., Horimasu, Y., Miyamoto, S., Iwamoto, H., Fujitaka, K., Miyata, Y., Miyake, M., Kohno, N., Okada, M., Hattori, N., 2018. Aminopeptidase N/CD13 as a potential therapeutic target in malignant pleural mesothelioma. Eur. Respir. J. 51, 1701610. https://doi.org/10.1183/13993003.01610-2017.

Pasqualini, R., Koivunen, E., Kain, R., Lahdenranta, J., Sakamoto, M., Stryhn, A., Ashmun, R.A., Shapiro, L.H., Arap, W., Ruoslahti, E., 2000. Aminopeptidase N is a receptor for tumor-homing peptides and a target for inhibiting angiogenesis. Cancer Res. 60, 722–727.

Rundhaug, J.E., 2005. Matrix metalloproteinases and angiogenesis. J. Cell. Mol. Med. 9, 267–285. https://doi.org/10.1111/j.1582-4934.2005.tb00355.x.

Satpati, D., Sharma, R., Kumar, C., Sarma, H.D., Dash, A., 2017. ^{68}Ga-Chelation and comparative evaluation of *N*,*N*'-bis-[2-hydroxy-5-(carboxyethyl)benzyl]ethylenediamine-*N*,*N*'-diacetic acid (HBED-CC) conjugated NGR and RGD peptides as tumor targeted molecular imaging probes. MedChemComm. 8, 673-679. https://doi.org/10.1039/c7md00006e.

Satpati, D., Sharma, R., Sarma, H.D., Dash, A., 2018. Comparative evaluation of 68 Ga-labeled NODAGA, DOTAGA, and HBED-CC-conjugated cNGR peptide chelates as tumor-targeted molecular imaging probes. Chem. Biol. Drug Des. 91, 781-788. https://doi.org/10.1111/cbdd.13143.

Schreiber, C.L., Smith, B.D., 2018. Molecular Imaging of Aminopeptidase N in Cancer and Angiogenesis. Contrast Media Mol. Imaging. 2018, 5315172. https://doi.org/10.1155/2018/5315172.

Shao, Y., Liang, W., Kang, F., Yang, W., Ma, X., Li, G., Zong, S., Chen, K., Wang, J., 2014a. ^{68}Ga-Labeled Cyclic NGR Peptide for MicroPET Imaging of CD13 Receptor Expression. Molecules. 19, 11600-11612. https://doi.org/10.3390/molecules190811600.

Shao, Y., Liang, W., Kang, F., Yang, W., Ma, X., Li, G., Zong, S., Chen, K., Wang, J., 2014b. A direct comparison of tumor angiogenesis with ^{68}Ga-labeled NGR and RGD peptides in HT-1080 tumor xenografts using microPET imaging. Amino Acids. 46, 2355-2364. https://doi.org/10.1007/s00726-014-1788-x.

Teleanu, R.I., Chircov, C., Grumezescu, A.M., Teleanu, D.M., 2019. Tumor Angiogenesis and Anti-Angiogenic Strategies for Cancer Treatment. J. Clin. Med. 9, 84. https://doi.org/10.3390/jcm9010084.

Trencsenyi, G., Marian, T., Bako, F., Emri, M., Nagy, G., Kertai, P., Banfalvi, G., 2014. Metastatic hepatocarcinoma he/de tumor model in rat. J. Cancer. 5, 548-558. https://doi.org/10.7150/jca.9315.

Trencsényi, G., Dénes, N., Nagy, G., Kis, A., Vida, A., Farkas, F., Szabó, J.P., Kovács, T., Berényi, E., Garai, I., Bai, P., Hunyadi, J., Kertész, I., 2017. Comparative preclinical evaluation of (68)Ga-NODAGA and (68)Ga-HBED-CC conjugated procainamide in melanoma imaging. J. Pharm. Biomed. Anal. 139, 54-64. https://doi.org/10.1016/j.jpba.2017.02.049.

Vats, K., Satpati, D., Sharma, R., Kumar, C., Sarma, H.D., Dash, A., 2017. ^{99m} Tc-labeled NGR-chlorambucil conjugate, ^{99m} Tc-HYNIC-CLB-c(NGR) for targeted chemotherapy and molecular imaging. J. Labelled Comp. Radiopharm. 60, 431-438. https://doi.org/10.1002/jlcr.3522.

Vats, K., Satpati, A.K., Sharma, R., Sarma, H.D., Satpati, D., Dash, A., 2018. ^{177}Lu-labeled cyclic Asn-Gly-Arg peptide tagged carbon nanospheres as tumor targeting radio-nanoprobes. J. Pharm. Biomed. Anal. 152, 173-178. https://doi.org/10.1016/j.jpba.2018.01.052.

Wu, C., Li, F., Niu, G., Chen, X., 2013. PET imaging of inflammation biomarkers. Theranostics. 3, 448−466. https://doi.org/10.7150/thno.6592.

Zhang, J., Lu, X., Wan, N., Hua, Z., Wang, Z., Huang, H., Yang, M., Wang, F., 2014. 68Ga-DOTA-NGR as a novel molecular probe for APN-positive tumor imaging using

MicroPET. Nucl. Med. Biol. 41, 268−275. https://doi.org/10.1016/j.nucmedbio.2013.12.008.

Zheng, Y.B., Gong, J.H., Liu, X.J., Li, Y., Zhen, Y.S., 2017. A CD13-targeting peptide integrated protein inhibits human liver cancer growth by killing cancer stem cells and suppressing angiogenesis. Mol. Carcinog. 56, 1395-1404. https://doi.org/10.1002/mc.22600.

Zou, M., Zhang, L., Xie, Y., Xu, W., 2012. NGR-based strategies for targeting delivery of chemotherapeutics to tumor vasculature. Anticancer Agents Med. Chem. 12, 239-246. https://doi.org/10.2174/187152012800228751.